Median and Radius-Driven Interval Uncertainty Modeling for Security-Constrained Economic Dispatch

Xiaohong Ran, *Member, IEEE*, Siqi Bu, *Senior Member, IEEE*

***Abstract*—The diverse uncertainties from renewable energy sources and loads make the security-constrained economic dispatch (SCED) problem more challenging. Inaccuracies in interval uncertainty models lead to overly conservative scheduling results. This paper proposes an interval modeling method from median and radius, using their respective uncertainties to characterize the randomness of an interval. Given multiple uncertain sources, a joint probability distribution is developed, followed by the construction of an uncertain interval and probability- driven Conditional Value at Risk (CVaR). A grid security indicator is proposed to represent the operating state of the power grid, with the line having the smallest security margin determining the overall security level. Furthermore, a multi-period SCED is developed, incorporating system security and reserve regulation through the uncertain interval and probability-driven CVaR method. Notably, the security margin is integrated into the SCED model as both an objective and a constraint. Security and reserve constraints are transformed into deterministic linear forms using the uncertain interval and probability-driven CVaR, reducing computational complexity while accurately reflecting the influence of various random sources on SCED. Case studies demonstrate the effectiveness and scalability of the proposed risk evaluation method and SCED model.**

***Index Terms*—Security-constrained economic dispatch, security margin, uncertain interval, conditional value at risk.**

NOMENCLATURE

A. Parameters

N_g, N_w	Number of thermal units and wind farms.
N_d, N_l	Number of bus loads and lines.
$P_{gi}^{\max}$, $P_{gi}^{\min}$	Maximal/minimal powers of the ith thermal unit.
$P_{wj}^{\max}$, $P_{wj}^{\min}$	Maximal/minimal powers of the jth wind farm.
a_{gi},b_{gi},c_{gi}	Coefficients of generation cost for the ith unit.
M_1, N_1	Wind power median and radius sample number in security margin loss function.
M_2, N_2	Wind power median and radius sample number in reserve regulation loss function.
K_1, K_2	Load sample number in security margin loss and reserve regulation loss functions.
$\mathbf{B}_L$,$\mathbf{B}_N$	Susceptance matrix of the lines and buses.
$\mathbf{H}_C$	Node-branch incidence matrix, indicating the connection between nodes and branches.
$\widetilde{\boldsymbol{P}}_{w,t}^{f}$	Forecasted wind power interval at time t.
$\boldsymbol{P}_{w,t}^{f-}$, $\boldsymbol{P}_{w,t}^{f+}$	Lower and upper limits of forecasted wind power.
$\mu_{w,r}$, $\sigma_{w,r}$	Mean value and standard deviation of radius.
μ_d, σ_d	Mean value and standard deviation of bus load.
$R_{u,i}$, $R_{d,i}$	Ramp-up/down limits of the ith thermal unit.
$\widetilde{\boldsymbol{\delta}}$	Unit interval with [-1,1].
β_1, β_2	Confidence levels of security margin and reserve.
C_s^+, C_s^-	Coefficients of up and down reserve regulation loss.
C_m^+	Coefficient of security margin loss.
δw, $\delta \rho$	Coefficients of wind power and load reserves.
a_i, b_i	Lower and upper limits of Uniform distribution U.
$P_{wi,t}^{cl}$, $P_{wi,t}^{cu}$	Lower and upper limits of the ith median.
γ	Security margin of a power system.

B. Variables

$P_{gi,t}$	Power generation of the ith traditional unit at time t.
$\boldsymbol{P}_{int,t}$	Bus inject power at time t.
$\boldsymbol{P}_{d,t}$, $\boldsymbol{P}_{d,t}^{f}$	Vectors of actual and forecasted nodal active power loads.
$\boldsymbol{P}_{g,t}$	Vector of traditional generator at time t.
$\widetilde{\boldsymbol{P}}_{w,t}$	Actual wind power interval at time t.
$\boldsymbol{P}_{w,t}^{-}$, $\boldsymbol{P}_{w,t}^{+}$	Lower and upper limits of actual wind power.
$\boldsymbol{P}_{w,t}^{c}$, $\boldsymbol{P}_{w,t}^{r}$	Interval median and radius of wind generation.
α_1, α_2	VaRs of security margin and reserve regulation.
P_{ij}^{L}, $P_{ij}^{L,\max}$	Normal and maximal power flows of line ij.
$\mathrm{z}_{ij}^{\mathrm{marg}}$	Security margin of active power of line ij.
$h_m(.)$	Probabilistic distribution of median at time t.
$h_r(.)$	Probabilistic distribution of radius at time t.
$h_{mr}(.)$	Joint distribution of median and radius at time t.
$h(.)$	Joint distribution of median, radius, load at time t.

C. Abbreviations

CCED	Chance-constrained economic dispatch.
CIP-CVaR	Correlated interval and probabilistic-based CVaR.
CVaR	Conditional value-at-risk.
FDIA	False data injection attack.
IMP	Interval median and probability.
IP-CVaR	Interval and probabilistic-based CVaR.
IRVs	Interval random variables.
PDFs	Probability density functions.
PRVs	Probabilistic random variables.
RES	Renewable energy sources.
SCED	Security-constrained economic dispatch.
UPFC	Unified power flow controller.

I. Introduction

A. Relevant Research

As global climate change accelerates, the integration of Renewable Energy Sources (RES) into power systems is rapidly increasing [1, 2]. Renewable power generation reduces reliance on traditional thermal power, but its uncertainty and intermittency significantly impact the stability [3, 4] and secure operation of power systems [5, 6]. Other sources of uncertainty include controllable and interruptible loads, as well as random outages of thermal generators and transformers [7]. These unpredictable

This work was supported by the Hong Kong Research Grant Council for the Research Project under Grants 15208323. Paper no. TPWRS-01959-2024. *(Corresponding author: Siqi Bu.)*

Xiaohong Ran is with the Department of Electrical and Electronic Engineering, The Hong Kong Polytechnic University, Kowloon, Hong Kong, (e-mail: xiaohong.ran@polyu.edu.hk).

Siqi Bu is with the Department of Electrical and Electronic Engineering, Shenzhen Research Institute, Research Centre for Grid Modernisation, Research Institute for Smart Energy, Policy Research Centre for Innovation and Technology, International Centre of Urban Energy Nexus, and Centre for Advances in Reliability and Safety, The Hong Kong Polytechnic University, Kowloon, Hong Kong (e-mail: siqi.bu@polyu.edu.hk).

fluctuations of RES and other random factors can lead to line overloads or load shedding under extreme operating conditions. To address the challenges caused by multiple uncertainties, the Security-Constrained Economic Dispatch (SCED) aims to minimize production costs while satisfying the operational and security constraints of power grids [8]. Various SCED strategies have been proposed to robustly and economically manage power system variability.

Recently, SCED has been extensively modeled and studied in [9 - 17]. A measurement-based method for real-time SCED was introduced in [9], where the proposed approach showed robustness against inaccurate model parameters and system disturbances. In [10], the SCED problem was addressed using cardinality minimization, and a continuous difference-of-convex approximation was developed. To manage the nonlinearity and nonconvexity of incorporating the Unified Power Flow Controller (UPFC) into SCED, a novel UPFC model and its convexification were developed [11], significantly reducing the computational burden. In [12] and [13], the energy and ancillary services were studied in network-constrained electricity markets, and the reserve cost and line security constraints were considered in the proposed model. Moreover, a zonal reserve modeling was proposed in a co-optimized energy and reserve market [14], allocating the zonal total transfer capability between energy and reserves in an economic way. However, these prior studies exhibit two limitations: (1) they overlook the stochastic nature of RES and its cascading impacts on reserve capacity, and economic operation; (2) the adopted constraints are modeled deterministically. The scheduling flexibility is limited and results are conservative. Moreover, a low-carbon SCED model has been developed to promote carbon neutrality. The computational complexity of SCED was reduced using clustering methods and deep learning [15]. To compensate the variation of wind power, an SCED model integrating hybrid energy storage (pumped hydro and battery systems) has been developed. However, the established optimization scheduling model was a deterministic optimization [16]. Additionally, stochastic dispatch modeling was introduced in [17] using joint chance constraint approximations, but power system security was not considered.

Current research on RES uncertainty includes robust optimization, stochastic optimization, and interval optimization. First, robust optimization is a key method for solving SCED models. In previous work [18], a multi-period SCED model incorporating RES was proposed using distributionally robust optimization to account for random operating costs. The proposed approach avoided overly conservative solutions in the presence of inaccurate uncertainty data and significantly reduced average operating costs. A distributed SCED model utilizing blockchain technology was also studied [19]. Hierarchical and blockchain consensus algorithms were utilized to ensure accurate SCED modes against malicious behavior. Additionally, a segmented distributionally robust optimization for ED was introduced [20], and a difference-of-convex optimization was used to handle bilinear constraints. However, security concerns were not thoroughly addressed in the ED formulation. In addition to RES-related SCED challenges, False Data Injection Attacks (FDIAs) on SCED were also investigated, including financially motivated FDIAs [21] and a distributed robust ED scheme [22]. Robust optimization provides feasible and mathematically tractable solutions by considering uncertainty sets. However, the resulting decisions tend to be overly conservative, as the method typically focuses on worst-case scenarios.

In contrast, stochastic optimization offers another approach to model RES uncertainty and can more accurately represent its impact on SCED. In [23], a stochastic SCED was presented by considering the wind power uncertainty, where the probability distribution of wind power was established and Monte Carlo simulation was used to capture its stochastic nature. The Chance-Constrained Economic Dispatch (CCED) was also introduced to handle RES uncertainties, including two-sided CCED [24] and data-driven joint CCED [25]. In this case, the chance-constrained approach was utilized to describe RES uncertainty and its varying inequality constraints on power grids. To better quantify the influence of random factors or risks in ED, the Conditional Value-at-Risk (CVaR) method was introduced. The CVaR method was originally developed in the field of financial investment [26]. With the increasing integration of RES, the CVaR method has become widely adopted in the power sector to characterize the impact of RES uncertainty on grid security and operation. A distributed risk-averse optimal dispatch model was proposed for the integrated power and transportation system [27], where the CVaR method was used to characterize risks related to power load, RES, transportation demand, and carbon trading. Moreover, a joint probability distribution of wind, solar, and load was proposed in [28], and their combined effect on ED was analyzed in detail. Additionally, multi-timescale dispatch [29] and day-ahead dispatch for flexible traction power supply systems [30] were proposed, both employing the CVaR method to accurately model RES uncertainty in risk-related costs. However, the probability distribution of different uncertainties is not always accurately obtainable due to data loss or other predicted errors.

Recently, interval optimization has attracted significant attention for its ability to address challenges arising from interval uncertainty. Regarding RES interval uncertainty, an interval-based evaluation of available transfer capability in power grids was conducted in [31], and a central limit theorem-based power flow computation was proposed in [32]. However, the power flow results in [32] were obtained through interval variable optimization, where uncertainty was represented solely by fixed upper and lower bounds, without a precise probability distribution. Additionally, a multi-objective optimal dispatch model based on interval optimization was initially solved using a chaotic group search optimizer with multiple producers [33], and later via deep reinforcement learning [34]. However, in the above method, the interval boundary is treated as a decision variable rather than a random variable.

With the increasing complexity of uncertainty types, including probabilistic and interval randomness, two key questions arise: First, how can interval randomness be constructed and characterized. Second, how can risk assessment be conducted when interval and probabilistic randomness coexist. Existing research [35, 36] have made valuable contributions to interval modeling and risk assessment under the coexistence of interval and probabilistic randomness. Specifically, the Interval and Probabilistic-based CVaR (IP-CVaR) method [35] and the Correlated Interval and Probabilistic-based CVaR (CIP-CVaR) approach [36] were proposed. In [35], a joint distribution of interval and probabilistic random variables was established, while [36] introduced a method for modeling correlations among interval variables. However, interval modeling remains in its early stages, as existing models still represent intervals using fixed boundaries rather than treating them as random variables. In [37], a risk-averse robust interval ED model was proposed; however, it still required the probability distribution of wind power. Consequently, its applicability is limited. A recent

study on interval randomness [38] has provided momentum for further interval modeling development. In this study, the median's randomness, derived from the central limit theorem, is modeled using a uniform distribution. This approach retains interval randomness while accommodating extreme scenarios with unknown probability distributions, mirroring traditional probability methods in flexibility. However, a limitation in the Affine algorithm used in [38] is that interval radius is modeled as a fixed value, failing to reflect its inherent randomness. Moreover, the above ED model does not account for the impact of interval and probabilistic randomness on risk loss and power system security.

B. Motivation and Contribution

Therefore, modeling interval uncertainty and capturing the joint impact of multiple uncertain sources on the SCED model remains a technical challenge. This challenge forms the primary motivation of this paper. Additionally, we aim to further develop a power grid security indicator and examine how interval and probabilistic random variables affect secure grid operation. Addressing the aforementioned research gaps in security and economic dispatch, this paper presents four key innovations: (1) the construction of uncertain interval, (2) a novel risk assessment method, (3) a line security margin indicator, and (4) a novel SCED model. These contributions are detailed as follows:

(1) The construction of random interval model. This paper proposes a novel interval modeling method driven by median and radius, improving upon traditional models. The model separately establishes the probability distributions of the median and radius, along with their joint distribution, to more accurately capture interval randomness.

(2) A novel risk assessment method. Based on the traditional deterministic interval-probability CVAR, this paper proposes an uncertain interval and probability-based CVaR. The proposed method uses the probability distributions of the median and radius to more accurately estimate risk losses from probabilistic and interval uncertainties, thereby reducing the conservatism caused by traditional risk assessment methods.

(3) A line security margin indicator of a power grid. A security indicator is proposed to evaluate the state of the power grid. In the proposed indicator, the line with the smallest security margin determines the overall security level of the grid. In other words, if the line with the smallest security margin meets operating constraints, the system is considered secure. Otherwise, it is deemed unsafe.

(4) A novel SCED considering multiple uncertain sources. This paper proposes a new SCED framework that captures risk losses from both interval and probabilistic uncertainties in reserve regulation and security margins. The proposed interval and probability-driven CVaR transforms stochastic constraints into deterministic forms, reducing complexity while accurately reflecting the influence of various uncertainties.

The remainder of the paper is organized as follows. Section II establishes the security margin indicator for power systems, while Section III introduces the economic and security models for power systems. In Section IV, the novel SCED is proposed, and Section V presents the case study. Finally, the conclusion is presented in Section VI.

II. Security Margin of Power Systems

Transmission line capacity is typically incorporated into the SCED model using inequality constraints. However, this paper focuses on assessing line security risks and associated cost losses caused by various uncertainties. Therefore, the first step is to establish the power grid's security domain under the combined influence of probabilistic and interval uncertainties. Next, the remaining capacity of each line is determined, and the overall grid security margin is defined to support the development of security risk loss models.

A. Security Domain of Power Systems

The security operating model of power systems is constrained by various equality and inequality conditions. Given an operating boundary of a power grid, its security operating domain $\mathbf{\Gamma}_1$ is mathematically defined in Eq. (1).

$$\mathbf{\Gamma}_1 = \begin{Bmatrix} \boldsymbol{u} | f(\boldsymbol{x}, \boldsymbol{u}) = 0 \\ \mathrm{z}(\boldsymbol{x}, \boldsymbol{u}) \leq 0 \end{Bmatrix} \tag{1}$$

Here $\boldsymbol{x} \in \mathbf{R}^n$ and $\boldsymbol{u} \in \mathbf{R}^m$ denote the state and control variables, respectively. The functions f and z represent all equality and inequality constraints of power grids.

With increasing demand for electric load and the integration of large amounts of renewable energy into power systems, various random variables, including Probabilistic Random Variables (PRVs) and Interval Random Variables (IRVs), are considered in optimizing power grid operating [35]. Here, the PRV is represented by $\boldsymbol{\xi} = (\xi_1, \xi_2, ..., \xi_K)$ and the IRV is similarly denoted by $\widetilde{\boldsymbol{\zeta}} \in [\boldsymbol{\zeta}^L, \boldsymbol{\zeta}^U]$, where $\boldsymbol{\zeta}^L$ and $\boldsymbol{\zeta}^U$ are lower and upper limits of $\widetilde{\boldsymbol{\zeta}}$. Accordingly, the security domain $\mathbf{\Gamma}_2$ with PRV and IRV can be described as follows

$$\mathbf{\Gamma}_2 = \begin{Bmatrix} \boldsymbol{u} | f(\boldsymbol{x}, \boldsymbol{u}, \boldsymbol{\xi}, \widetilde{\boldsymbol{\zeta}}) = 0 \\ \mathrm{z}(\boldsymbol{x}, \boldsymbol{u}, \boldsymbol{\xi}, \widetilde{\boldsymbol{\zeta}}) \leq 0 \end{Bmatrix} \tag{2}$$

If the Jacobian matrix of $f(\boldsymbol{x}, \boldsymbol{u}, \boldsymbol{\xi}, \widetilde{\boldsymbol{\zeta}})$ is not singular, then state variable can also be represented by: $\boldsymbol{x} = \boldsymbol{x}(\boldsymbol{u}, \boldsymbol{\xi}, \widetilde{\boldsymbol{\zeta}})$. Substituted $\boldsymbol{x}$ into the $\mathrm{z}(\boldsymbol{x}, \boldsymbol{u}, \boldsymbol{\xi}, \widetilde{\boldsymbol{\zeta}})$, accordingly, the inequality constraints can be described as follows

$$\mathrm{z}(\boldsymbol{x}(\boldsymbol{u}, \boldsymbol{\xi}, \widetilde{\boldsymbol{\zeta}}), \boldsymbol{u}, \boldsymbol{\xi}, \widetilde{\boldsymbol{\zeta}}) \leq 0 \tag{3}$$

Here, we define a novel function $Z(\boldsymbol{u}, \boldsymbol{\xi}, \widetilde{\boldsymbol{\zeta}})$:

$$Z(\boldsymbol{u}, \boldsymbol{\xi}, \widetilde{\boldsymbol{\zeta}}) = \max_{1 \leq j \leq d} \mathrm{z}_j(\boldsymbol{y}, \boldsymbol{\xi}, \widetilde{\boldsymbol{\zeta}}) \tag{4}$$

where $Z(\boldsymbol{u}, \boldsymbol{\xi}, \widetilde{\boldsymbol{\zeta}})$ can be maximum value of $\mathrm{z}_j(\boldsymbol{u}, \boldsymbol{\xi}, \widetilde{\boldsymbol{\zeta}})$. d is the sampling number.

According to the description in Eq. (4), when the function $Z(\boldsymbol{u}, \boldsymbol{\xi}, \widetilde{\boldsymbol{\zeta}}) \leq 0$, the security domain $\mathbf{\Gamma}_2$ illustrated in Eq. (2) can be described as follows

$$\mathbf{\Gamma}_2 = \begin{Bmatrix} \boldsymbol{u} | f(\boldsymbol{x}, \boldsymbol{u}, \boldsymbol{\xi}, \widetilde{\boldsymbol{\zeta}}) = 0 \\ \max\limits_{1 \leq j \leq d} \mathrm{z}_j(\boldsymbol{u}, \boldsymbol{\xi}, \widetilde{\boldsymbol{\zeta}}) \leq \varrho < 0 \end{Bmatrix} \tag{5}$$

Here ϱ is a negative number approaching 0.

Inspired by the general operating domain $\mathbf{\Gamma}_2$ described in Eq. (5), the next subsection we discuss how to establish the security constraints in terms of transmission line for power systems.

B. Security Margin of Power Systems

Given the maximum transmission capacity $P_{ij}^{L,\max}$ of line ij, the security constraint of line between bus i and j generally is represented in Eq. (6).

$$|P_{ij}^L| \leq P_{ij}^{L,\max} \tag{6}$$

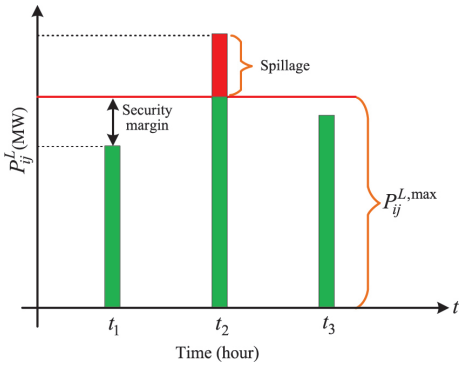

Fig. 1. Schematic diagram of security margin in a power system.

To facilitate the characterization of the remaining capacity of different lines, given line active power P_{ij}^{L}, the security margin $\mathrm{z}_{ij}^{\mathrm{marg}}$ is modeled in Eq. (7), shown in Fig. 1.

$$\mathrm{z}_{ij}^{\mathrm{marg}} = \frac{P_{ij}^{L,\max} - |P_{ij}^{L}|}{P_{ij}^{L,\max}} \tag{7}$$

As described in Eq. (7), different line has a various security margin. The transmission line with the smallest security margin determines the security level of entire power system. In other words, if the line with the smallest security margin meets operating constraints, the power grid operates safely. Therefore, the security margin level is defined as follows

$$\min_{ij\in N_l} \mathrm{z}_{ij}^{\mathrm{marg}} = \min_{ij\in N_l} \left\{ \frac{P_{ij}^{L,\max} - |P_{ij}^{L}|}{P_{ij}^{L,\max}} \right\} \tag{8}$$

Here, the line capacity P_{ij}^{L} is a state variable, which is a function of $\boldsymbol{P}_{g,t}$, $\boldsymbol{P}_{d,t}$ and $\widetilde{\boldsymbol{P}}_{w,t}$. Thus, the security margin of entire power system is denoted in Eq. (9).

$$\begin{aligned} \eta(\boldsymbol{P}_{g,t}, \widetilde{\boldsymbol{P}}_{w,t}, \boldsymbol{P}_{d,t}) &= \min_{ij\in N_l} \mathrm{z}_{ij}^{\mathrm{marg}}(\boldsymbol{P}_{g,t}, \widetilde{\boldsymbol{P}}_{w,t}, \boldsymbol{P}_{d,t}) \\ &= \min_{ij\in N_l} \frac{P_{ij}^{L,\max} - |P_{ij}^{L}|}{P_{ij}^{L,\max}} \end{aligned} \tag{9}$$

Eq. (10) describes the inequality constraint for system security. We know if the line power flow satisfies Eq. (10), the power system operates securely; otherwise, it is in an insecure state.

$$\min_{ij\in N_l} \left\{ \frac{P_{ij}^{L,\max} - |P_{ij}^{L}|}{P_{ij}^{L,\max}} \right\} \geq 0 \tag{10}$$

Given the variety and number of random variables considered in this paper, we use a DC model to calculate the line power flow, described as follows

$$\begin{aligned} P_{ij}^{L} &= \mathbf{B}_L \mathbf{H}_C \mathbf{B}_N \boldsymbol{P}_{int,t} \\ \boldsymbol{P}_{int,t} &= \boldsymbol{P}_{g,t} + \widetilde{\boldsymbol{P}}_{w,t} - \boldsymbol{P}_{d,t} \end{aligned} \tag{11}$$

Substituted Eq. (11) into Eq. (10), accordingly, Eq. (10) can be rewritten as follows

$$\min_{ij\in N_l} \left\{ \frac{P_{ij}^{L,\max} - |\mathbf{B}_L \mathbf{H}_C \mathbf{B}_N \boldsymbol{P}_{int,t}|}{P_{ij}^{L,\max}} \right\} \geq 0 \tag{12}$$

Line power flow changes are driven by bus injection power, including traditional generators, wind generations, and loads. The injection power of traditional generators is deterministic, while wind power and load are random variables that significantly affect line power flows. This study examines how the power flow of transmission lines is affected by IRVs and PRVs.

III. CVaR-Based Security Margin and Reserve Regulation

To accurately characterize the impact of interval randomness on power grid security and cost losses, this paper introduces median- and radius-based random models to construct a corresponding random interval model. Based on probabilistic and interval uncertainty models, we construct loss functions for both security margin and reserve regulation, and apply the CVaR method to characterize the relationship between different types of randomness and associated cost losses.

A. Introduction of Interval Random Variables

As discussed in [35] and [36], wind power has been modeled as an interval random variable (IRV) due to data loss or predicted errors. According to [32], the interval median $\boldsymbol{P}_{w,t}^{c}$ follows a uniform distribution, which was used in [38] to construct an uncertain interval model termed Interval Median and Probability (IMP)-based risk evaluation. Currently, modeling IRVs faces two major challenges: the resulting intervals are often too large, leading to conservative estimates, and the inherent randomness of IRVs remains insufficiently explored. Therefore, random interval modeling remains an open research problem.

Specifically, the actual wind power interval can be modeled as: $\tilde{\boldsymbol{P}}_{w,t} = \boldsymbol{P}_{w,t}^{c} \oplus (\boldsymbol{P}_{w,t}^{r} \odot \widetilde{\boldsymbol{\delta}}) = [\boldsymbol{P}_{w,t}^{c} - \boldsymbol{P}_{w,t}^{r}, \boldsymbol{P}_{w,t}^{c} + \boldsymbol{P}_{w,t}^{r}]$. This paper discusses intervals from the median and radius, using their respective uncertainty to characterize the randomness of an interval. Fig. 2 illustrates the relationship between actual and predicted power intervals. Similar to the Probability Density Function (PDF)-based approaches, the predicted error of the interval-based method is evaluated based on the relative positions of actual and predicted intervals, denoted by $\left[\boldsymbol{P}_{w,t}^{-}, \boldsymbol{P}_{w,t}^{+}\right]$ and $\left[\boldsymbol{P}_{w,t}^{f-}, \boldsymbol{P}_{w,t}^{f+}\right]$, respectively. A sectional view of an IRV is shown in Fig. 3, with the maximum interval represented as $\left[\boldsymbol{P}_{w,t}^{\min}, \boldsymbol{P}_{w,t}^{\max}\right]$.

B. Median and Radius-driven Uncertain Interval

Due to data loss and other predicted errors, the wind power is treated as an IRV. Here, a median and radius-driven interval model of wind power generation is shown in Fig. 3. Accordingly, the uncertainty of an interval is characterized by the respective uncertainties of median and radius. Here, we know the interval median in [38] was modeled using a Uniform distribution.

$$h_m(P_{wi,t}^{c}) = \begin{cases} \dfrac{1}{b_i - a_i}, & a_i \leq P_{wi,t}^{c} \leq b_i \\ 0, \quad \text{others.} \end{cases} \tag{13}$$

where the median follows Uniform distribution, and $P_{wi,t}^{c} \sim U(P_{wi,t}^{cl}, P_{wi,t}^{cu})$.

From [35], if the interval radius is modeled as a constant value, the proposed method not only has a limited application range, but also has a strong conservative calculation result. Thus, the interval radius should be also modeled as a random variable. In [39, 40], the Gaussian distribution was used to simulate the wind power predicted error. Compared with PDF-based method [39, 40], discussed separately, the upper and lower boundary power predicted error of interval-based method also follows normal distribution [41]. Moreover, the radius of an interval is equal to $\left(\boldsymbol{P}_{w,t}^{+} - \boldsymbol{P}_{w,t}^{-}\right)/2$, which is linear to the upper and lower bounds of an interval. Therefore, according to the central limit theorem, the predicted error of the interval radius still follows the normal

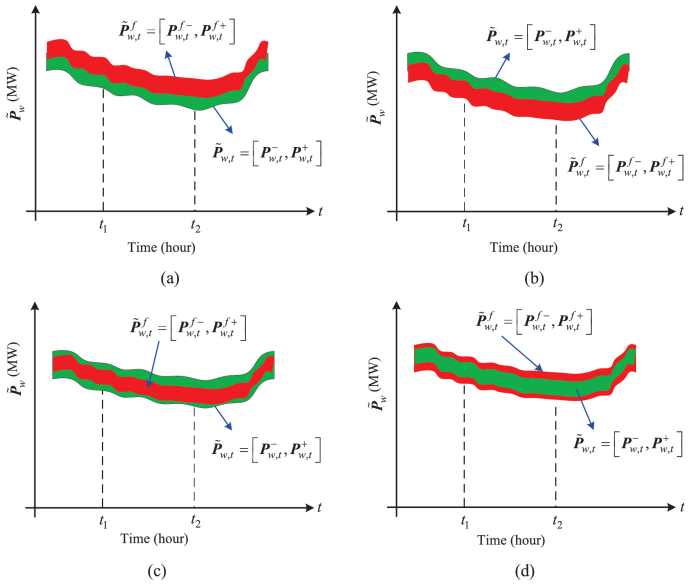

Fig. 2. Positional relationship between actual and predicted interval of wind power: (a) predicted interval limits are higher than the actual interval limits, (b) actual interval limits are higher than the predicted interval limits, (c) predicted interval is a subset of actual interval, i.e., $\tilde{\boldsymbol{P}}^{f}_{w,t} \subset \tilde{\boldsymbol{P}}_{w,t}$, (d) actual interval is a subset of predicted interval, i.e., $\tilde{\boldsymbol{P}}_{w,t} \subset \tilde{\boldsymbol{P}}^{f}_{w,t}$.

distribution. Accordingly, we establish the probability model of radius using normal distribution as follows

$$h_r(P^r_{wj,t}) = \frac{1}{\sqrt{2\pi}\sigma_{w,r}} \exp\left[-\frac{(P^r_{wj,t} - \mu_{w,r})^2}{2\sigma^2_{w,r}}\right]. \tag{14}$$

Here $P^r_{wj,t} \sim N(\mu_{w,r}, \sigma_{w,r})$, $\mu_{w,r} = (P^{f+}_{wj,t} - P^{f-}_{wj,t})/2$, and $\sigma_{w,r} = \kappa \cdot \mu_{w,r}$. $0 \le \kappa \le 1$.

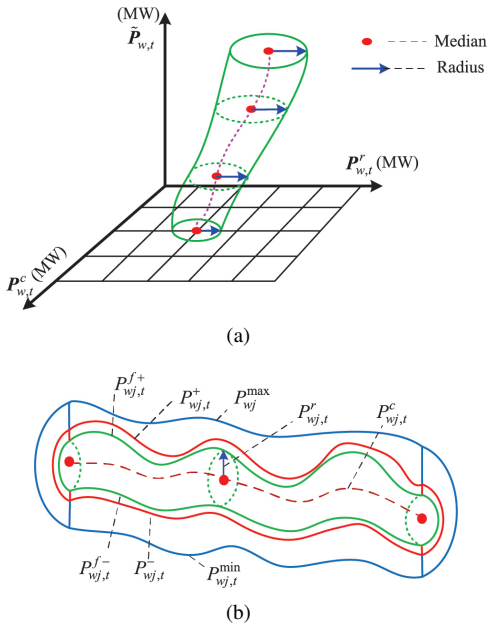

Fig. 3. Schematic diagram of interval uncertainty model: (a) interval described using median and radius, (b) sectional view of an interval.

Consequently, a stochastic model, i.e., joint probability distribution, of wind power generation is described from interval median and radius as follows

$$h_{mr}(P^c_{wj,t}, P^r_{wj,t}) = \begin{cases} \kappa_1 \cdot \exp\left[-\dfrac{(P^r_{wj,t} - \mu_{w,r})^2}{2\sigma^2_{w,r}}\right], & \forall t \\ 0, \quad \text{others} \end{cases} \tag{15}$$

Here $\kappa_1 = \frac{1}{b_i - a_i} \frac{1}{\sqrt{2\pi}\sigma_{w,r}}$.

In a power system with integration of renewable energy, aside from wind power uncertainty, the randomness of load is also considered, which follows a Gaussian distribution [6, 35].

$$h_d(P_{dk,t}) = \frac{1}{\sqrt{2\pi}\sigma_d} \exp\left[-\frac{(P_{dk,t} - \mu_d)^2}{2\sigma^2_d}\right], \ \forall t. \tag{16}$$

Therefore, considering the influence of wind power and load on the security operating of power system, the joint probability distribution of wind power and electric load is represented by

$$\begin{aligned} h(\boldsymbol{P}^c_{w,t}, \boldsymbol{P}^r_{w,t}, \boldsymbol{P}_{d,t}) &= h_{mr}(\boldsymbol{P}^c_{w,t}, \boldsymbol{P}^r_{w,t}) \cdot h_d(\boldsymbol{P}_{d,t}) \\ &= \begin{cases} \kappa_2 \cdot \exp\left[\dfrac{(\boldsymbol{P}^r_{w,t} - \mu_{w,r})^2}{2\sigma^2_{w,r}} + \dfrac{(\boldsymbol{P}_{d,t} - \mu_d)^2}{2\sigma^2_d}\right], \forall t \\ 0, \quad \text{others} \end{cases} \end{aligned} \tag{17}$$

Here $\kappa_2 = \frac{1}{b_i - a_i} \frac{1}{\sqrt{2\pi}\sigma_{w,r}} \frac{1}{\sqrt{2\pi}\sigma_d}$.

C. Security Margin Loss Based on CVaR

To effectively analyze the influence of multiple sources on the power grid security margin, considering the combined effect of IRVs and PRVs, we first establish a risk evaluation method, termed uncertain interval and probability-driven CVaR. The CVaR theory was originally proposed for the risk probability in the field of economics [26]. The risk-related functions are categorized as cost- function where lower values indicate better performance. As shown in Eq. (12), the power grid security margin represents a benefit-function where higher values correspond to enhanced system security. To ensure methodological consistency, the loss function characterizing power grid security margin is transformed into a cost-function, as described in the constraints section of SCED. Here, $\varphi(\boldsymbol{P}_{g,t}, \boldsymbol{P}^c_{w,t}, \boldsymbol{P}^r_{w,t}, \boldsymbol{P}_{d,t})$ is assumed to represent the loss function of security margin. The probability of $\Psi(\boldsymbol{P}_{g,t}, \alpha_1)$ not exceed a specified threshold α_1 is given by

$$\Psi(\boldsymbol{P}_{g,t}, \alpha_1) = \iiint_{\Omega_1} h(\boldsymbol{u}, \boldsymbol{v}, \boldsymbol{w}) d\boldsymbol{u} d\boldsymbol{v} d\boldsymbol{w} \tag{18}$$

Here $\Omega_1 = \{\varphi(\boldsymbol{P}_{g,t}, \boldsymbol{P}^c_{w,t}, \boldsymbol{P}^r_{w,t}, \boldsymbol{P}_{d,t}) \le \alpha_1\}$, and $\Psi(\boldsymbol{P}_{g,t}, \alpha_1)$ denotes the cumulative distribution function for the security margin loss.

It is worth mentioning that uncertain interval and probability-driven VaR, i.e., VaR_1, for the security margin at any confidence level β_1 is defined as follows

$$\mathrm{VaR}_1 = \min\left\{\alpha_1 \in \mathbb{R}, \ \Psi(\boldsymbol{P}_{g,t}, \alpha_1) \ge \beta_1\right\} \tag{19}$$

Based on the definition of uncertain interval and probability-driven CVaR, it is greater than the VaR. The higher the confidence level, the larger the CVaR is. Accordingly, the system security margin CVaR_1 can be defined as follows

$$\begin{aligned} \mathrm{CVaR}_1 &= \frac{1}{1-\beta_1} \iiint_{\Omega_2} H_1(\boldsymbol{P}_{g,t}, \boldsymbol{u}, \boldsymbol{v}, \boldsymbol{w}) d\boldsymbol{u} d\boldsymbol{v} d\boldsymbol{w} \\ H_1(\boldsymbol{P}_{g,t}, \boldsymbol{P}^c_{w,t}, \boldsymbol{P}^r_{w,t}, \boldsymbol{P}_{d,t}) &= \\ &\varphi(\boldsymbol{P}_{g,t}, \boldsymbol{P}^c_{w,t}, \boldsymbol{P}^r_{w,t}, \boldsymbol{P}_{d,t}) \cdot h(\boldsymbol{P}^c_{w,t}, \boldsymbol{P}^r_{w,t}, \boldsymbol{P}_{d,t}) \end{aligned} \tag{20}$$

where $\Omega_2 = \{\varphi(\boldsymbol{P}_{g,t}, \boldsymbol{P}^c_{w,t}, \boldsymbol{P}^r_{w,t}, \boldsymbol{P}_{d,t}) \ge \mathrm{VaR}_1\}$.

Due to the difficulty of calculating Eq. (20), a sampling based method is adopted. Therefore, given a confidence level β_1, the security margin CVaR_1 is reformulated in Eq. (21).

$$\begin{aligned}\mathrm{CVaR}_1 &= \mathrm{VaR}_1 + \frac{1}{1-\beta_1}\sum_{m=1}^{M_1}\sum_{n=1}^{N_1}\sum_{k=1}^{K_1}[\varphi - \mathrm{VaR}_1]^+ \\ &[\varphi(\boldsymbol{P}_{g,t}, P^c_{w,m}, P^r_{w,n}, P_{d,k}) - \mathrm{VaR}_1]^+ = \max(\varphi - \mathrm{VaR}_1, 0)\end{aligned} \tag{21}$$

Here $P^c_{w,m}$, $P^r_{w,n}$ and $P_{d,k}$ denote the mth, nth and kth random sampling points of wind power median, radius and load.

D. Reserve Regulation Loss Based on CVaR

After discussing power system security, we proceed to study spinning reserve regulation caused by wind power generation and electric load. Wind power is treated as an IRV due to data loss or other predicted errors. The relationship between actual power interval $[\boldsymbol{P}^-_{w,t}, \boldsymbol{P}^+_{w,t}]$ and predicted power interval $[\boldsymbol{P}^{f-}_{w,t}, \boldsymbol{P}^{f+}_{w,t}]$ can be illustrated in Fig. 2. According to the relative position of actual and predicted intervals, the wind power is given by

$$\boldsymbol{P}_{w,t} = \begin{cases} \boldsymbol{P}'_{w,t} = \boldsymbol{P}^c_{w,t} + \boldsymbol{P}^r_{w,t}, \ \boldsymbol{P}_{w,t} > \boldsymbol{P}^{f+}_{w,t}, \ \forall t \\ \boldsymbol{P}''_{w,t} = 0, \ \ \boldsymbol{P}_{w,t} \in \left[\boldsymbol{P}^{f-}_{w,t}, \boldsymbol{P}^{f+}_{w,t}\right] \\ \boldsymbol{P}'''_{w,t} = \boldsymbol{P}^c_{w,t} - \boldsymbol{P}^r_{w,t}, \ \boldsymbol{P}_{w,t} < \boldsymbol{P}^{f-}_{w,t} \end{cases} \tag{22}$$

Similar, the electric load can be described in Eq. (23).

$$\boldsymbol{P}_{d,t} = \begin{cases} \boldsymbol{P}'_{d,t}, \ \boldsymbol{P}_{d,t} > \boldsymbol{P}^f_{d,t}, \ \forall t \\ \boldsymbol{P}''_{d,t}, \ \boldsymbol{P}_{d,t} < \boldsymbol{P}^f_{d,t} \end{cases} \tag{23}$$

Overestimating wind power raises positive reserve. So the positive spinning reserve regulation cost is modeled in Eq. (24).

$$h_1(\boldsymbol{P}_{g,t}, \boldsymbol{P}^c_{w,t}, \boldsymbol{P}^r_{w,t}, \boldsymbol{P}_{d,t}) = C^+_s \cdot \left[\begin{array}{l} \sum_{j=1}^{N_w}\left[P^{f-}_{wj,t} - P'''_{wj,t}\right]^+ \\ + \sum_{k=1}^{N_d}\left[P'_{dk,t} - P^f_{dk,t}\right]^+ \end{array} \right] \tag{24}$$

Similar, underestimating wind power generation increases negative reserve. The negative spinning reserve regulation cost is then defined in Eq. (25).

$$h_2(\boldsymbol{P}_{g,t}, \boldsymbol{P}^c_{w,t}, \boldsymbol{P}^r_{w,t}, \boldsymbol{P}_{d,t}) = C^-_s \cdot \left[\begin{array}{l} \sum_{j=1}^{N_w}\left[P'_{wj,t} - P^{f+}_{wj,t}\right]^+ \\ + \sum_{k=1}^{N_d}\left[P^f_{dk,t} - P''_{dk,t}\right]^+ \end{array} \right] \tag{25}$$

Hence, total spinning reserve regulation loss cost is described in Eq. (26).

$$\begin{aligned}\phi(\boldsymbol{P}_{g,t}, \boldsymbol{P}^c_{w,t}, \boldsymbol{P}^r_{w,t}, \boldsymbol{P}_{d,t}) &= h_1(\boldsymbol{P}_{g,t}, \boldsymbol{P}^c_{w,t}, \boldsymbol{P}^r_{w,t}, \boldsymbol{P}_{d,t}) \\ &+ h_2(\boldsymbol{P}_{g,t}, \boldsymbol{P}^c_{w,t}, \boldsymbol{P}^r_{w,t}, \boldsymbol{P}_{d,t})\end{aligned} \tag{26}$$

Given the loss function of reserve regulation, the probability of $\Phi(\boldsymbol{P}_{g,t}, \alpha_2)$ not exceed a threshold α_2 is described as

$$\Phi(\boldsymbol{P}_{g,t}, \alpha_2) = \iiint_{\Omega_3} h(\boldsymbol{u}, \boldsymbol{v}, \boldsymbol{w}) d\boldsymbol{u} d\boldsymbol{v} d\boldsymbol{w} \tag{27}$$

Here $\Omega_3 = \{\phi(\boldsymbol{P}_{g,t}, \boldsymbol{P}^c_{w,t}, \boldsymbol{P}^r_{w,t}, \boldsymbol{P}_{d,t}) \le \alpha_2\}$. $\Phi(\boldsymbol{P}_{g,t}, \alpha_2)$ represents the cumulative distribution function for reserve regulation.

Given the confidence level β_2 in (0,1), the VaR_2 for the reserve regulation loss is given by

$$\mathrm{VaR}_2 = \min\left\{\alpha_2 \in \mathbb{R}, \ \Phi(\boldsymbol{P}_{g,t}, \alpha_2) \ge \beta_2\right\} \tag{28}$$

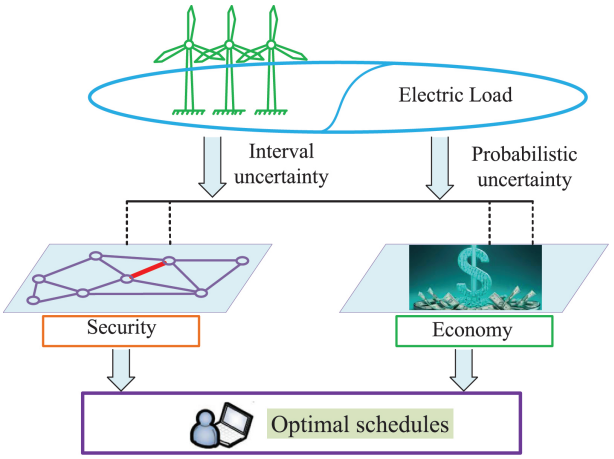

Fig. 4. Diagram on security and economy.

Accordingly, the reserve regulation loss CVaR_2 is represented by

$$\begin{aligned}\mathrm{CVaR}_2 &= \frac{1}{1-\beta_2}\iiint_{\Omega_4} H_2(\boldsymbol{P}_{g,t}, \boldsymbol{u}, \boldsymbol{v}, \boldsymbol{w}) d\boldsymbol{u} d\boldsymbol{v} d\boldsymbol{w} \\ H_2(\boldsymbol{P}_{g,t}, \boldsymbol{P}^c_{w,t}, \boldsymbol{P}^r_{w,t}, \boldsymbol{P}_{d,t}) &= \\ &\phi(\boldsymbol{P}_{g,t}, \boldsymbol{P}^c_{w,t}, \boldsymbol{P}^r_{w,t}, \boldsymbol{P}_{d,t}) \cdot h(\boldsymbol{P}^c_{w,t}, \boldsymbol{P}^r_{w,t}, \boldsymbol{P}_{d,t})\end{aligned} \tag{29}$$

Here $\Omega_4 = \{\phi(\boldsymbol{P}_{g,t}, \boldsymbol{P}^c_{w,t}, \boldsymbol{P}^r_{w,t}, \boldsymbol{P}_{d,t}) \ge \mathrm{VaR}_2\}$.

Using sampling techniques, the reserve regulation described in Eq. (30) is rewritten as follows

$$\begin{aligned}\mathrm{CVaR}_2 &= \mathrm{VaR}_2 + \frac{1}{1-\beta_2}\sum_{m=1}^{M_2}\sum_{n=1}^{N_2}\sum_{k=1}^{K_2}[\phi - \mathrm{VaR}_2]^+ \\ &[\phi(\boldsymbol{P}_{g,t}, P^c_{w,m}, P^r_{w,n}, P_{d,k}) - \mathrm{VaR}_2]^+ = \max(\phi - \mathrm{VaR}_2, 0)\end{aligned} \tag{30}$$

The reformulations in Eqs. (21) and (30) quantify the expected security margin and reserve regulation losses in power systems. Furthermore, the newly added constraints are linear, making them computationally efficient and easy to implement. The complete mathematical formulation is presented in the following section.

IV. Proposed Security-constrained Economic Dispatch

This section presents the objective function of the proposed SCED model. In addition to traditional deterministic constraints, the model incorporates risk constraints for line security and reserve, which are reformulated as deterministic constraints using the proposed CVaR method.

A. Objective Function

Considering power generation cost, line overload penalty and reserve costs, the objective function of proposed SCED during dispatch period T is given by

$$\begin{aligned}\min \ Z = &\sum_{t=1}^{T}\sum_{i=1}^{N_g} F_g(P_{gi,t}) + \sum_{t=1}^{T} F_{\beta_1}(\boldsymbol{P}^c_{w,t}, \boldsymbol{P}^r_{w,t}, \boldsymbol{P}_{d,t}, \alpha_1) \\ &+ \sum_{t=1}^{T} F_{\beta_2}(\boldsymbol{P}^c_{w,t}, \boldsymbol{P}^r_{w,t}, \boldsymbol{P}_{d,t}, \alpha_2)\end{aligned} \tag{31}$$

In Eq. (31), the first term denotes the generation cost, the second term corresponds to the overload penalty cost quantifying the risk loss of exceeding line capacity limits, and the third term

accounts for the reserve regulation cost. The generation cost of conventional generators is modeled using a quadratic function.

$$F_g(P_{gi,t}) = a_{gi}P_{gi,t}^2 + b_{gi}P_{gi,t} + c_{gi} \tag{32}$$

While emphasizing power system security, the model also considers economic efficiency. A diagram illustrating the relationship between security and economy is shown in Fig. 4. According to Eq. (21), the sub-objective function for bearing RES-induced line overload risk loss at confidence level β_1 is reformulated as follows

$$\begin{aligned} &F_{\beta_1}(\boldsymbol{P}_{w,t}^c, \boldsymbol{P}_{w,t}^r, \boldsymbol{P}_{d,t}, \alpha_1) = \alpha_1 + \frac{1}{1-\beta_1}\sum_{m=1}^{M_1}\sum_{n=1}^{N_1}\sum_{k=1}^{K_1}[\mathrm{z}_{1mnk}]^+ \\ &\text{s.t.} \qquad \mathrm{z}_{1mnk} = \varphi(\boldsymbol{P}_{g,t}, P_{w,m}^c, P_{w,n}^r, P_{d,k}) - \alpha_1 \end{aligned} \tag{33}$$

Similarly, another sub-objective function for spinning reserve regulation cost at confidence level β_2 is defined in Eq. (34), based on Eq. (30).

$$\begin{aligned} &F_{\beta_2}(\boldsymbol{P}_{w,t}^c, \boldsymbol{P}_{w,t}^r, \boldsymbol{P}_{d,t}, \alpha_2) = \alpha_2 + \frac{1}{1-\beta_2}\sum_{m=1}^{M_1}\sum_{n=1}^{N_1}\sum_{k=1}^{K_1}[\mathrm{z}_{2mnk}]^+ \\ &\text{s.t.} \qquad \mathrm{z}_{2mnk} = \phi(\boldsymbol{P}_{g,t}, P_{w,m}^c, P_{w,n}^r, P_{d,k}) - \alpha_2 \end{aligned} \tag{34}$$

The equality and inequality constraints of the proposed SCED model, as well as the risk constraints of above two loss functions will be introduced below.

B. Deterministic Constraints

(1) Power balance constraint

$$\sum_{i=1}^{N_g} P_{gi,t} + \sum_{j=1}^{N_w} \tilde{P}_{wj,t}^f = \sum_{k=1}^{N_d} P_{dk,t}, \forall t \tag{35}$$

(2) Upper and lower limits of generator output

$$P_{gi}^{\min} \le P_{gi,t} \le P_{gi}^{\max}, i = 1, 2..., N_g \tag{36}$$

(3) Ramp constraints

$$\begin{aligned} -R_{d,i} \le P_{gi,t} - P_{gi,t-1}, \\ P_{gi,t} - P_{gi,t-1} \le R_{u,i}, \ \forall i, t \end{aligned} \tag{37}$$

(4) Positive reserve constraint

$$\begin{aligned} &\sum_{i=1}^{N_g} P_{gi,t}^{su} \ge \sum_{j=1}^{N_w} P_{wj,t}^d \times \delta w + \sum_{k=1}^{N_d} P_{dk,t} \times \delta\rho \\ &P_{gi,t}^{su} = \min\left\{(P_{gi}^{\max} - P_{gi,t}), \ R_{u,i}T_{10}\right\} \end{aligned} \tag{38}$$

Here $P_{wj,t}^d = \mathbb{E}[P_{wj,t}^{f-} - P_{wj,t}^{'''}]$. $\mathbb{E}$ is an expectation operator, and T_{10} denotes 10 minutes.

(5) Negative reserve constraint

$$\begin{aligned} &\sum_{i=1}^{N_g} P_{gi,t}^{sd} \ge \sum_{j=1}^{N_w} P_{wj,t}^u \times \delta w + \sum_{k=1}^{N_d} P_{dk,t} \times \delta\rho \\ &P_{gi,t}^{sd} = \min\left\{(P_{gi,t} - P_{gi}^{\min}), \ R_{d,i}T_{10}\right\} \end{aligned} \tag{39}$$

Here $P_{wj,t}^u = \mathbb{E}[P_{wj,t}^{'} - P_{wj,t}^{f+}]$.

(6) Wind power generation constraints

$$\begin{aligned} &P_{wj}^{\min} \le \tilde{P}_{wj,t}^f \le P_{wj}^{\max} \\ &\tilde{P}_{wj,t} = [P_{wj,m}^c - P_{wj,n}^r, P_{wj,m}^c + P_{wj,n}^r] \\ &P_{wj}^{\min} \le \tilde{P}_{wj,t} \le P_{wj}^{\max} \\ &j = 1, 2..., N_w \end{aligned} \tag{40}$$

Constraints (40) illustrate the forecasted and actual ranges of wind power generation are both limited to its rated range.

C. Risk Constraints

(1) Transmission line security constraints

The transmission line security constraint is typically formulated as $|P_{ij}^L| \le P_{ij}^{L,\max}$. However, the large-scale integration of wind power significantly impacts line security. To address this issue, a chance constraint (as shown in Eq. (41)) is introduced to limit the risk of line overloading while accommodating wind power uncertainties.

$$\Pr\left(-P_{ij}^{L,\max} \le P_{ij}^L \le P_{ij}^{L,\max}\right) \ge \beta_1 \tag{41}$$

While Eq. (41) theoretically imposes security constraints on all lines, the system operation reveals that grid security is principally governed by the critical branch operating closest to its limit. Eq. (42) is established to limit line overloads.

$$\Pr\left\{\max_{ij\in N_l}\left[C_m^+ \cdot (|P_{ij}^L| - P_{ij}^{L,\max}), 0\right] \le \gamma\right\} \ge \beta_1 \tag{42}$$

To enable computationally tractable risk assessment, this paper characterizes the chance-constraint Eq. (42) using uncertain interval and probability-driven CVaR method, mathematically represented as F_{β_1}. The F_{β_1} is constrained not only by security margin γ, but also by the CVaR-related constraints.

$$\begin{aligned} &F_{\beta_1} = \alpha_1 + \frac{1}{1-\beta_1}\sum_{m=1}^{M_1}\sum_{n=1}^{N_1}\sum_{k=1}^{K_1}[\mathrm{z}_{1mnk}]^+ \le \gamma \\ &\mathrm{z}_{1mnk} \ge \varphi(\boldsymbol{P}_{g,t}, P_{w,m}^c, P_{w,n}^r, P_{d,k}) - \alpha_1 \\ &\mathrm{z}_{1mnk} \ge 0 \\ &\varphi(\boldsymbol{P}_{g,t}, P_{w,m}^c, P_{w,n}^r, P_{d,k}) = \max_{ij\in N_l}\left[C_m^+ \cdot (|P_{ij}^L| - P_{ij}^{L,\max}), 0\right] \\ &m = 1, 2..., M_1, n = 1, 2, ..., N_1, k = 1, 2, ..., K_1 \end{aligned} \tag{43}$$

(2) CVaR-based reserve regulation constraints

The randomness of wind power affects both the secure operation of transmission lines and system reserves. Therefore, the CVaR-related constraints associated with reserve regulation loss F_{β_2} must also be satisfied.

$$\begin{aligned} &\mathrm{z}_{2mnk} \ge \phi(\boldsymbol{P}_{g,t}, P_{w,m}^c, P_{w,n}^r, P_{d,k}) - \alpha_2 \\ &\mathrm{z}_{2mnk} \ge 0 \\ &m = 1, 2..., M_2 \\ &n = 1, 2, ..., N_2 \\ &k = 1, 2, ..., K_2 \end{aligned} \tag{44}$$

By applying the proposed CVaR method, this study converts stochastic constraints into deterministic ones, simplifying the solution of the subsequent optimization models.

Since the proposed SCED is an interval optimization model, it is transformed into two ordinary optimization problems, namely, upper and lower limit models. According to previous studies [35, 42], the lower bound model is established when the actual interval equals the predicted interval and the predicted wind power assumes its upper bound. Similarly, the upper bound model is constructed when the actual interval exceeds the predicted interval and the predicted wind power assumes its lower bound. For further details, refer to [35, 42].

Consequently, a security-based risk dispatch that considers the combined impact of IRVs and PRVs has been developed. The model analyzes both the security and economic performance of power systems and offers a practical dispatch strategy for grid operators. The risk model is solved using the fmincon optimization solver in the Matlab toolbox, and the flow chart of the proposed framework is illustrated in Fig. 5.

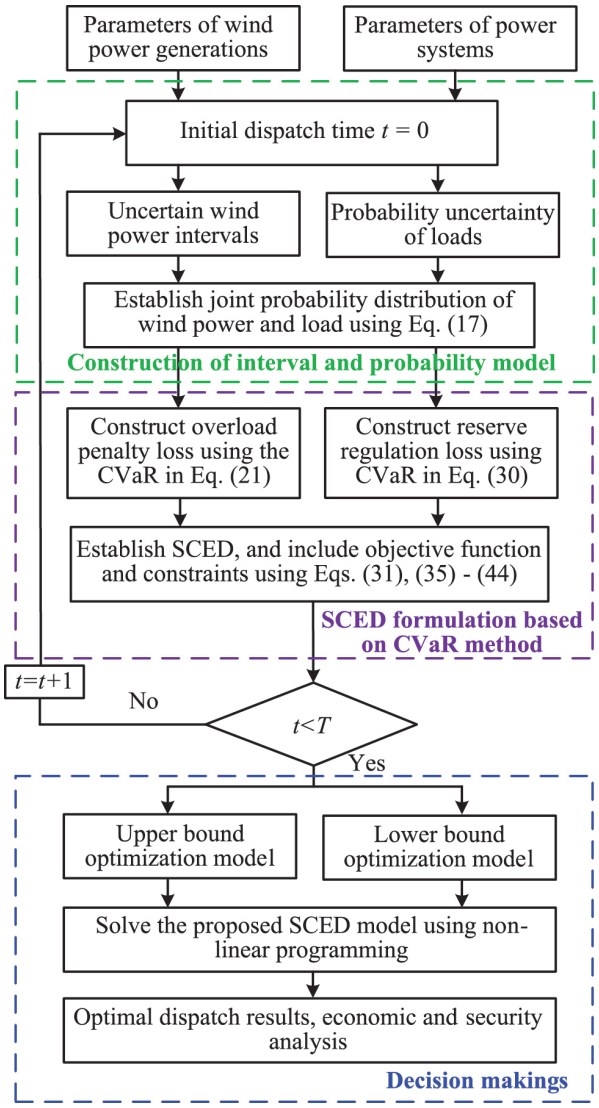

Fig. 5. Flow chart of the proposed SCED.

V. Case Study

The performance of the proposed SCED is evaluated using MATLAB. Simulation results for the IEEE-39, 118 and 300 bus power systems are presented using a PC with a 12th Gen Intel(R) Core(TM) i5-12500H 2.50 GHz processor, 16.0 GB RAM, and MATLAB 2021b.

A. Results of the Proposed CVaR-based SCED Model

IEEE-39 test system consists of ten units, three wind farms, and 46 branches. Three wind farms are integrated at buses 8, 22, and 26, with maximum capacities set to 100 MW each. The cost coefficients of positive and negative SRs are assumed to be C_s^+ = \$60(MW/h), and C_s^- = \$ 40(MW/h), respectively. The security level of the power grid is set to γ=1600, T = 2, δw=0.70, and C_m^+ = \$ 100(MW/h). In this case, the line capacity limit is set to 1.5 times the normal flow, and the load and wind power data are provided in [38]. The results are shown in Table I and II, respectively.

Table I presents the upper limit results at different confidence levels (β_1 and β_2). As shown in Table I, when the confidence level of reserve regulation β_1 equals that of system security β_2, (e.g., β_1 = β_2 = 0.92, 0,94, 0.96, 0.98), both reserve and total costs increase with β_1 and β_2. However, the generation and overload penalty costs remain unchanged at \$36199.332 and \$612.305, respectively. When the confidence level $\beta_1 \neq \beta_2$, both total and reserve regulation costs still increase with rising confidence levels.

TABLE I
Upper limit results under different confidence levels (\$)

Confidence level	Generation cost	Reserve cost	Total cost
$\beta_1 = \beta_2 = 0.92$	36199.332	5330.687	42142.324
$\beta_1 = \beta_2 = 0.94$	36199.332	5589.223	42400.860
$\beta_1 = \beta_2 = 0.96$	36199.332	5864.616	42676.253
$\beta_1 = \beta_2 = 0.98$	36199.332	6190.329	43001.966
$\beta_1 = 0.92, \beta_2 = 0.98$	36199.332	5526.698	42338.335
$\beta_1 = 0.94, \beta_2 = 0.98$	36199.332	5957.083	42768.720
$\beta_1 = 0.96, \beta_2 = 0.98$	36199.332	6034.786	42846.423

TABLE II
Lower limit results under different confidence levels (\$)

Confidence level	Generation cost	Reserve cost	Total cost
$\beta_1 = \beta_2 = 0.92$	35510.694	4047.054	41157.748
$\beta_1 = \beta_2 = 0.94$	35510.694	4251.428	41362.123
$\beta_1 = \beta_2 = 0.96$	35510.694	4520.320	41631.014
$\beta_1 = \beta_2 = 0.98$	35510.694	4881.680	41992.375
$\beta_1 = 0.92, \beta_2 = 0.94$	35510.694	4047.054	41157.748
$\beta_1 = 0.92, \beta_2 = 0.96$	35510.694	4047.054	41157.748
$\beta_1 = 0.92, \beta_2 = 0.98$	35510.694	4047.054	41157.748
$\beta_1 = 0.94, \beta_2 = 0.92$	35510.694	4251.428	41362.123
$\beta_1 = 0.94, \beta_2 = 0.96$	35510.694	4251.428	41362.123
$\beta_1 = 0.94, \beta_2 = 0.98$	35510.694	4251.428	41362.123
$\beta_1 = 0.96, \beta_2 = 0.92$	35510.694	4520.320	41631.014
$\beta_1 = 0.96, \beta_2 = 0.94$	35510.694	4520.320	41631.014
$\beta_1 = 0.96, \beta_2 = 0.98$	35510.694	4520.320	41631.014

Table II presents the lower limit results, as $\beta_1 = \beta_2 = 0.92, 0.94, 0.96$ and 0.98, the total cost increases with rising confidence levels β_1 and β_2. When $\beta_1 \neq \beta_2$, (e.g., β_1 =0.92, β_2 =0.94), the lower limit total cost is approximately \$ 41157.748. As the confidence level β_2 increase from 0.94 to 0.98, the lower boundary total cost remains at \$ 41157.748. This is because the lower limit total cost is not affected by fluctuations of wind generation. Additionally, when β_2 =0.98, as the confidence level β_1 increases from 0.92 to 0.96, the lower limit total cost rises from \$ 41157.748 to \$ 41631.014. This increase in total cost is primarily due to the uncertainty of load. Confidence levels β_1 and β_2 are predetermined parameters rather than optimization variables. Their specific values should be determined by the dispatcher according to actual application scenarios. A higher confidence level is chosen for scenarios requiring greater reliability or security, and a lower one otherwise. Scheduling results under various confidence level combinations are presented in Tables I and II, demonstrating how scheduling outcomes vary with different confidence levels. These results provide an important reference for dispatchers to select appropriate confidence levels and develop practical scheduling strategies. Moreover, a higher confidence level typically results in more secure operation. However, achieving higher security requires more resources, leading to increased scheduling costs.

B. Performance Comparison of Proposed Evaluation Method with Benchmarks

This section discusses the performance comparison of the proposed method with benchmarks. The interval-based evaluation methods [31], [33], CIP-CVaR-based approach [36], and IMP-based risk evaluation method [38] are selected for comparison with the proposed approach. The upper limit results are shown in Table III and Fig. 6, while the lower limit dispatch results are presented in Table IV and Fig. 7. In Table III and IV, ρ represents the interval correlation coefficient.

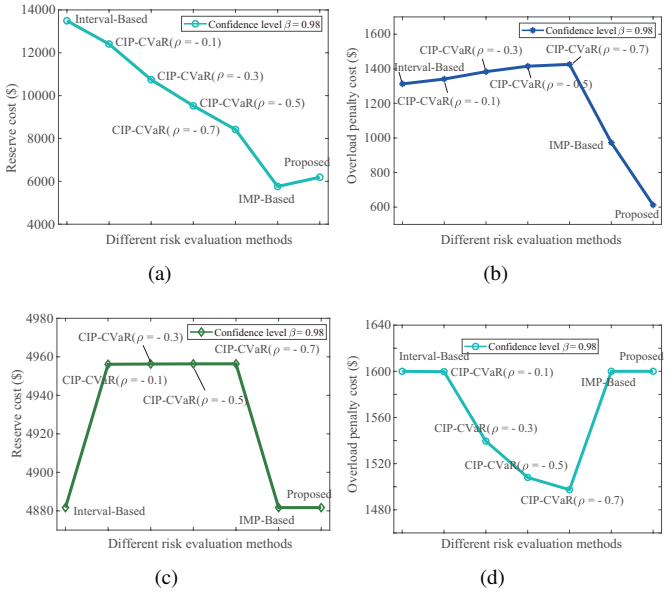

Fig. 6. Comparison of results from different methods: (a) upper limit reserve cost, (b) upper limit overload penalty cost, (c) lower limit reserve cost, (d) lower limit overload penalty cost.

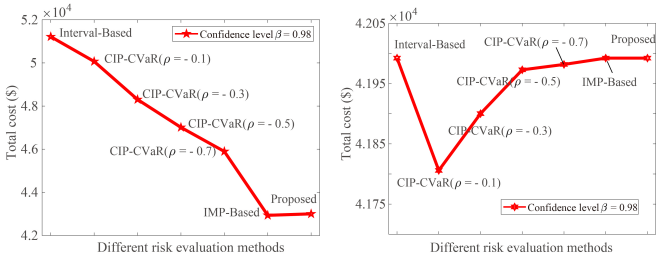

Fig. 7. Comparison of results from different methods: (a) upper limit total cost, (b) lower limit total cost.

TABLE III
COMPARISON OF UPPER LIMIT RESULTS OBTAINED BY DIFFERENT RISK EVALUATION METHODS ($)

Risk evaluation method	Reserve cost	Overload penalty cost	Total cost
Interval-based method	13492.354	1312.717	51216.985
CIP-CVaR$\|_{\rho=-0.1}$	12408.561	1340.600	50068.426
CIP-CVaR$\|_{\rho=-0.3}$	10743.938	1383.497	48304.241
CIP-CVaR$\|_{\rho=-0.5}$	9524.900	1414.955	47012.250
CIP-CVaR$\|_{\rho=-0.7}$	8416.746	1425.604	45895.147
IMP-based method	5761.661	973.056	42934.005
Proposed method	6190.329	612.305	43001.966

From Table III and Fig. 6, it is evident that the interval-based evaluation methods [31], [33], yields much larger upper limits than other risk evaluation methods. This is because the interval-based method adopts maximum interval range. Although the interval-based method is highly robust, the cost required under extreme conditions is excessively high. Compared to the CIP-CVaR-based model [36], a smaller upper bound is obtained. As shown in Table III and Fig. 6, interval correlation affects reserve regulation and system security. As the correlation increases, the upper limit of reserve cost decreases gradually, while overload penalty cost increases. Therefore, this CIP-CVaR-based method allows the dispatcher to address the influence of interval correlation on SCED reasonably and effectively. The IMP-based method [38] obtains a slightly smaller upper limit for total cost,

TABLE IV
COMPARISON OF LOWER LIMIT RESULTS OBTAINED BY DIFFERENT RISK EVALUATION METHODS ($)

Risk evaluation method	Reserve cost	Overload penalty cost	Total cost
Interval-based method	4881.680	1600.00	41992.375
CIP-CVaR$\|_{\rho=-0.1}$	4956.137	1599.717	41805.913
CIP-CVaR$\|_{\rho=-0.3}$	4956.274	1539.526	41900.232
CIP-CVaR$\|_{\rho=-0.5}$	4956.345	1508.068	41972.954
CIP-CVaR$\|_{\rho=-0.7}$	4956.369	1497.419	41981.892
IMP-based method	4881.680	1600.00	41992.375
Proposed method	4881.680	1600.00	41992.375

($ 42934.005 < $ 43001.966), compared with the proposed method. This is because the IMP-based risk evaluation [38] uses a constant interval radius, ignoring the uncertainty in the radius. Consequently, the proposed method overcomes the conservatism of traditional methods, yielding more reasonable and accurate results.

Compared to the interval-based and IMP-based methods [38], the proposed method achieves the same lower limit dispatch results, as shown in Table IV and Fig. 7. This is because the lower boundary cost is not affected by wind power uncertainty. For the CIP-CVaR-based method [36], the lower limit overload penalty cost decreases with rising interval correlation. Additionally, the reserve cost remains constant regardless of changes in interval correlation.

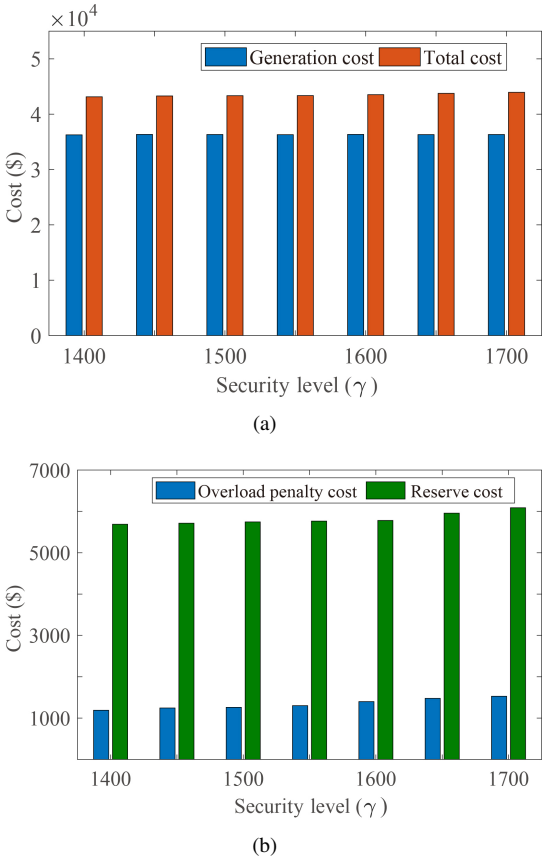

Fig. 8. Effect of different security levels on upper limit results: (a) generation and total costs, (b) overload penalty and reserve costs.

Regarding the computational complexity, we analyze it from the perspective of problem size and constraints. A comparative analysis of four different models is presented in Table V, where m and M denote the numbers of control and random variables, re-

TABLE V
COMPARATIVE ANALYSIS OF CALCULATION BURDEN

Methods	IP-CVaR method	CIP-CVaR approach	IMP-CVaR risk method	Proposed method
Number of control variable	m	m	m	$m+1+M$
Number of random variable	M	M	M	$2M$
Number of linear constraint	$2M$	$2M$	$2M$	$4M$
Notes	/	Dimension of correlation matrix	Uncertain median	Uncertain median and radius

spectively. Compared with the interval-based methods [31], [33], the CIP-CVaR method [36] is more computationally intensive due to the use of decorrelation techniques. Furthermore, both the IMP-based and the proposed risk evaluation methods require more complex sampling processes than the interval-based and CIP-CVaR methods, owing to the uncertain intervals. In the proposed method, the number of control variables increases by $1 + M$, including one variable (α_2) and an additional M variables introduced by the second CVaR-based loss function. Additionally, another $2M$ inequality constraints are introduced by the second loss function, thereby increasing the computational cost of the proposed model. The 250 LHS samples are taken as an example, the computational times for interval-based method [31], [33], CIP-CVaR approach [36], IMP-based risk evaluation [38], and the proposed approach are 138.02 s, 144.53 s, 146.32 s, and 161.69 s, respectively. Consequently, the proposed method has a slightly higher computational load than traditional methods. However, the dispatch results obtained by the proposed method are more accurate and reasonable.

C. Impact of Different Security Levels on Dispatch Results

This section examines the impact of various security levels on dispatch results. The parameters of the IEEE-39 test system are the same as those in Section A of the case study, and interval uncertainty in wind power is considered. The security levels of the transmission line are set to 1400, 1450, 1500,...,1700.

Fig. 8 illustrates the influence of different security levels on upper boundary dispatch results. In Fig. 8, the reserve and overload penalty costs rise as security level increases from 1400 to 1700. The maximum reserve and overload penalty costs are approximately \$ 6088.15024 and \$ 1528.9400. Finally, the upper limit of total cost rises from \$ 43138.9489 to \$ 43936.9558, and the power outputs of all generators during the dispatch period are shown in Fig. 9.

D. Impact of Wind Power Radius on Dispatch Results

This subsection examines the influence of wind power radius on dispatch results, validated on the IEEE-118 bus test system. Ten wind farms, each with a maximum capacity of 100 MW, are connected at buses 8, 22, 26, 35, 38, 51, 77, 88, 99, and 112. The operating parameters C_s^+ = \$60(MW/h), C_s^- = \$40(MW/h), γ=3000, and δw=0.70. To facilitate the quantitative analysis of subsequent research, the wind power range is redefined as follows: $\tilde{\boldsymbol{P}}_{w,t} = \boldsymbol{P}^c_{w,t} \oplus [(1-\lambda)\boldsymbol{P}^r_{w,t} \odot \widetilde{\boldsymbol{\delta}}]$. Here λ denotes the fluctuation range, and we list λ=0.2, 0.4, and 0.6 in this paper for comparative study. The dispatch results are shown in Fig. 10.

Fig. 10 describes the impact of wind power radius on the upper limit dispatch at different confidence level. As shown in Fig. 10, the reserve regulation cost gradually decreases as the parameter λ increases. A larger predicted interval increases the probability of random points falling within it, thereby reducing

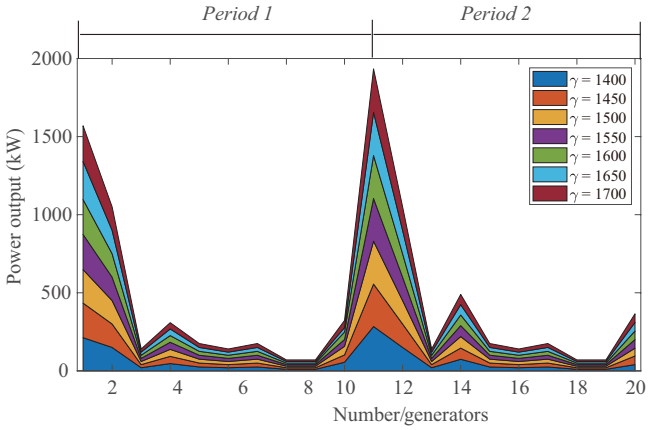

Fig. 9. Power outputs of all generator for different security levels.

the reserve regulation cost. (As noted in [35], random points within the forecasted interval do not incur reserve regulation costs). Additionally, as the confidence levels (β_1 and β_2) rise, both reserve cost and total cost increase to maintain secure operating of power grids. Therefore, the system scheduler must select confidence levels (β_1 and β_2) based on the required reliability of power system secure operating.

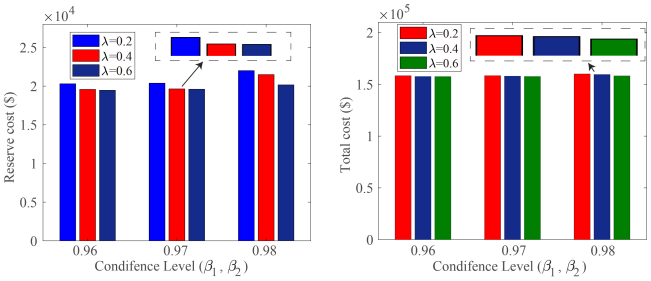

(a) (b)

Fig. 10. Effect of wind power radius on upper limit dispatch: (a) reserve cost, (b) total cost.

E. Impact of Wind Power Prediction on Security Margin

In this subsection, the IEEE 300-bus power system is employed to demonstrate the adaptability and scalability of the proposed SCED model. Ten wind farms are integrated at buses 28, 29, 106, 107, 112, 116, 163, 193, 194, and 204, each with a maximum capacity of 150 MW. The power grid security level is set to γ=10000, and other operating parameters are consistent with those of the IEEE 118-bus power system. The IEEE 300-bus system consists of 69 generators and 411 transmission lines. The line security dispatch results for the IEEE 300-bus system are shown in Fig. 11. To quantify the impact of wind power predicted on risk dispatch, the predicted upper and lower bounds of wind power are defined as follows

$$\begin{aligned} \boldsymbol{P}^u_{w,t} &= \boldsymbol{P}^{f+}_{w,t} + w\boldsymbol{P}^{f+}_{w,t} \\ \boldsymbol{P}^l_{w,t} &= \boldsymbol{P}^{f-}_{w,t} - w\boldsymbol{P}^{f-}_{w,t} \end{aligned} \tag{45}$$

where w represents the predicted deviation coefficient. $\boldsymbol{P}^u_{w,t}$ and $\boldsymbol{P}^l_{w,t}$ represent the upper and lower bounds of predicted wind power at time t, respectively.

According to the proposed SCED and risk evaluation method, Fig. 11 illustrates the line over-limit capacity at the first time period for w=0.18 and 0.22. The line over-limit capacity is defined as $\Delta P^L_{ij} = P^L_{ij} - P^{L,\max}_{ij}$. If ΔP^L_{ij}<0, the entire transmission

network is considered to be operating within the prescribed security margins. Otherwise, some line capacities exceed their maximum limits, indicating that the system is operating in an insecure state with potential stability risks. As shown in Fig. 11(c), five lines exceed their capacity limits: lines #13, #14, #59, #195, and #205. Among these, the maximum over-limit capacity is approximately 18.853 MW. When the predicted deviation coefficient is set to w=0.22, seven lines exceed the security limits: lines #13, #14, #59, #195, #205, #294, and #296, respectively. As shown in Fig. 11(d), the maximum over-limit capacity is 26.5591 MW on line # 195. Accordingly, the proposed SCED and risk assessment method can accurately characterize line security and its distribution under different wind power penetration scenarios. The proposed optimization method provides a valuable reference for power system dispatchers.

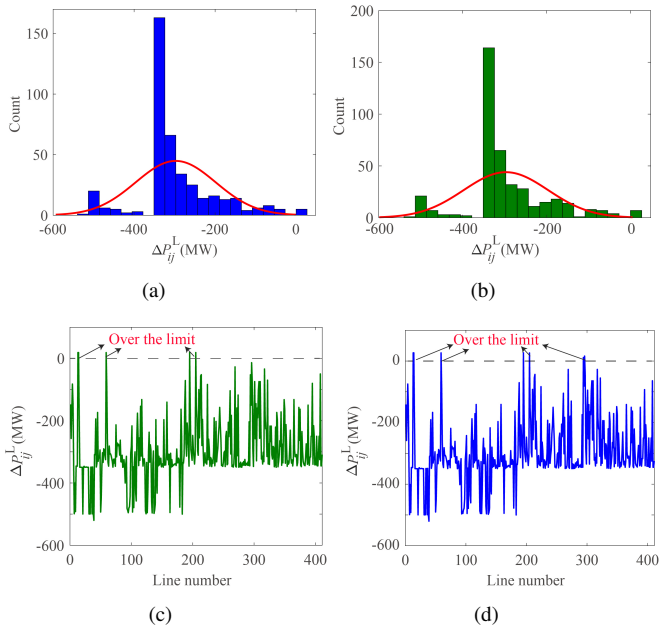

Fig. 11. Results of transmission line security on IEEE-300 bus power system: (a) statistical results of all lines at w=0.18, (b) line security distribution at w=0.22, (c) line capacities at w=0.18, (d) line capacities at w=0.22.

VI. Conclusion

This paper presents an interval uncertainty modeling method, and a novel multi-period CVaR-based SCED model. By considering the interval uncertainty of wind power and probabilistic uncertainty of electric load, we establish a joint probability distribution of multiple stochastic sources. The proposed model describes any uncertain interval through a combination of median and radius, using their respective uncertainty to characterize the randomness of an interval. It is concluded that the CVaR-based security margin can accurately assess the risk loss caused by multiple random sources. Additionally, the power generation, overload penalty and reserve costs are considered as dispatch objectives. The dispatch scheme achieves optimal generation cost while ensuring the security of power systems at various confidence levels. Compared with conventional SCED, the proposed model achieves more reasonable dispatch results, avoiding overly optimistic or conservative outcomes.

References

[1] X. Zhang, T. Ding, C. Mu, O. Han, *et al*, "Dual stochastic dual dynamic programming for multi-stage economic dispatch with renewable energy and thermal energy storage," *IEEE Trans. Power Syst.*, vol. 39, no. 2, pp. 3725 - 3737, Mar. 2024.

[2] Y. Chen and W. Wei, "Robust generation dispatch with strategic renewable power curtailment and decision-dependent uncertainty," *IEEE Trans. Power Syst.*, vol. 38, no. 5, pp. 4640 - 4654, Sep. 2023.

[3] S. Bu, J. Wen, and F. Li, "A generic framework for analytical probabilistic assessment of frequency stability in modern power system operational planning," *IEEE Trans. Power Syst.*, vol. 34, no. 5, pp. 3973 - 3976, Sep. 2019.

[4] Z. Wang and S. Bu, "Probabilistic analysis of small-signal stability of power systems affected by wind power generation uncertainties considering wake effects," *IEEE Trans. Power Syst.*, vol. 40, no. 2, pp. 1955 - 1968, Mar. 2025.

[5] Y. Wang, M. Xiao, Y. You, *et al*, "Optimized energy dispatch for microgrids with distributed reinforcement learning," *IEEE Trans. Smart Grid*, vol. 15, no. 3, pp. 2946 - 2956, May 2024.

[6] F. Fang, S. Yu, and X. Xin, "Data-driven-based stochastic robust optimization for a virtual power plant with multiple uncertainties," *IEEE Trans. Power Syst.*, vol. 37, no. 1, pp. 456 - 466, Jan. 2022.

[7] Z. Hu, Y. Xu, M. Korkali, *et al*, "A Bayesian approach for estimating uncertainty in stochastic economic dispatch considering wind power penetration," *IEEE Trans. Sustain. Energy*, vol. 12, no. 1, pp. 671 - 681, Jan. 2021.

[8] J. Hu, Y. Ye, Y. Tang, and G. Strbac, "Towards risk-aware real-time security constrained economic dispatch: a tailored deep reinforcement learning approach," *IEEE Trans. Power Syst.*, vol. 39, no. 2, pp. 3972 - 3986, Mar. 2024.

[9] K. Horn, A. Domínguez-García, and P. Sauer, "Measurement-based real-time security-constrained economic dispatch," *IEEE Trans. Power Syst.*, vol. 31, no. 5, pp. 3548 - 3560, Sep. 2016.

[10] D. Troxell, M. Ahn, and H. Gangammanavar, "A cardinality minimization approach to security-constrained economic dispatch," *IEEE Trans. Power Syst.*, vol. 37, no. 5, pp. 3642 - 3652, Sep. 2022.

[11] X. Wu, R. Wang, Y. Wang, and L. Wang, "A novel UPFC model and its convexification for security-constrained economic dispatch," *IEEE Trans. Power Syst.*, vol. 37, no. 6, pp. 4202 - 4213, Nov. 2022.

[12] T. Wu, M. Rothleder, Z. Alaywan, and A. D. Papalexopoulos, "Pricing energy and ancillary services in integrated market systems by an optimal power flow," *IEEE Trans. Power Syst.*, vol. 19, no. 1, pp. 339 - 347, Feb. 2004.

[13] J. M. Arroyo and F. D. Galiana, "Energy and reserve pricing in security and network constrained electricity markets," *IEEE Trans. Power Syst.*, vol. 20, no. 2, pp. 634 - 643, May 2005.

[14] T. Zheng and E. Litvinov, "Contingency-based zonal reserve modeling and pricing in a co-optimized energy and reserve market," *IEEE Trans. Power Syst.*, vol. 23, no. 2, pp. 277 - 286, May 2008.

[15] Z. Xu, X. Guan, H. Jiang, *et al*, "Carbon neutrality computational cost optimization for economic dispatch with carbon capture power plants in smart grid," *IEEE Trans. Sustain. Comput.*, vol. 9, no. 3, pp. 354 - 370, May/Jun. 2024.

[16] J. Li, S. Wang, L. Ye, and J. Fang, "A coordinated dispatch method with pumped-storage and battery-storage for compensating the variation of wind power," *Prot. Control Mod. Power Syst.*, vol. 3, no. 1, pp. 1 - 14, Jan. 2018.

[17] Y. Wen, Y. Guo, Z. Hu, and G. Hug, "Multiple joint chance constraints approximation for uncertainty modeling in dispatch problems," *IEEE Trans. Power Syst.*, vol. 40, no. 1, pp. 662 - 675, Jan. 2025.

[18] X. Lu, K. Chan, S. Xia, B. Zhou, *et al*, "Security-constrained multiperiod economic dispatch with renewable energy utilizing distributionally robust optimization," *IEEE Trans. Sustain. Energy*, vol. 10, no. 2, pp. 768 - 779, Apr. 2019.

[19] S. Chen, L. Zhang, Z. Yan, and Z. Shen, "A distributed and robust security-constrained economic dispatch algorithm based on blockchain," *IEEE Trans. Power Syst.*, vol. 37, no. 1, pp. 691 - 700, Jan. 2022.

[20] K. Qu, Y. Chen, S. Xie, X. Zheng, and J. Zhu, "Segmented distributionally robust optimization for real-time power dispatch with wind uncertainty," *IEEE Trans. Power Syst.*, vol. 39, no. 2, pp. 2970 - 2983, Mar. 2024.

[21] C. Liu, M. Zhou, J. Wu, *et al*, "Financially motivated FDI on SCED in real-time electricity markets: attacks and mitigation," *IEEE Trans. Smart Grid*, vol. 10, no. 2, pp. 1949 - 1959, Mar. 2019.

[22] B. Huang, Y. Li, F. Zhan, Q. Sun, and H. Zhang, "A distributed robust economic dispatch strategy for integrated energy system considering cyber-attacks," *IEEE Trans. Ind. Informat.*, vol. 18, no. 2, pp. 880 - 890, Feb. 2022.

[23] X. Zhu, Z. Yu, and X. Liu, " Security constrained unit commitment with extreme wind scenarios," *J. Mod. Power Syst. Clean Energy*, vol. 8, no. 3, pp. 464 - 472, May 2020.

[24] S. Xu and W. Wu, "Tractable reformulation of two-side chance-constrained economic dispatch," *IEEE Trans. Power Syst.*, vol. 37, no. 1, pp. 796 - 799, Jan. 2022.

[25] C. Wu and A. Kargarian, "Computationally efficient data-driven joint chance constraints for power systems scheduling," *IEEE Trans. Power Syst.*, vol. 38, no. 3, pp. 2858 - 2867, May 2023.

[26] R. Rockafellar and S. Uryasev, "Optimization of conditional value-at risk," *J. Risk*, vol. 2, no. 3, pp. 21 - 41, Oct. 2000.

[27] Z. Li, Q. Wu, H. Li, *et al*, " Distributed risk-averse optimal dispatch for integrated power and transportation system considering carbon trading," *IEEE Trans. Smart Grid*, vol. 15, no. 6, pp. 5583 - 5594, Nov. 2024.
[28] X. Ran, S. Miao, Z. Jiang, and H. Xu, "A framework for uncertainty quantification and economic dispatch model with wind-solar energy," *Int. J. Elect. Power Energy Syst.*, vol. 73, pp. 23 - 33, Dec. 2015.
[29] K. Wang, C. Wang, Z. Zhang, and X. Wang, "Multi-timescale active distribution network optimal dispatching based on SMPC," *IEEE Trans. Ind. Appl.*, vol. 58, no. 2, pp. 1644 - 1653, Mar./Apr. 2022.
[30] X. Wang, Y. Han, L. Li, *et al*, "CVaR quantitative uncertainty-based optimal dispatch for flexible traction power supply system," *IEEE Trans. Transport. Electrific.*, vol. 10, no. 1, pp. 1900 - 1910, Mar. 2024.
[31] X. Kou and F. Li, "Interval optimization for available transfer capability evaluation considering wind power uncertainty," *IEEE Trans. Sustain. Energy*, vol. 11, no. 1, pp. 250 - 259, Jan. 2020.
[32] C. Zhang, Q. Liu, B. Zhou, *et al*, "A central limit theorem-based method for dc and ac power flow analysis under interval uncertainty of renewable power generation," *IEEE Trans. Sustain. Energy*, vol. 14, no. 1, pp. 563 - 575, Jan. 2023.
[33] Y. Li, P. Wang, H. Gooi, *et al*, "Multi-objective optimal dispatch of microgrid under uncertainties via interval optimization," *IEEE Trans. Smart Grid*, vol. 10, no. 2, pp. 2046 - 2058, Mar. 2019.
[34] C. Mu, Y. Shi, N. Xu, *et al*, 'Multi-objective interval optimization dispatch of microgrid via deep reinforcement learning," *IEEE Trans. Smart Grid*, vol. 15, no. 3, pp. 2957 - 2970, May 2024.
[35] X. Ran, J. Zhang, and K. Liu, "An interval-probabilistic CVaR (IP-CVaR) and modelling for unknown probability distribution of some random variables," *IEEE Trans. Power Syst.*, vol. 38, no. 3, pp. 2035 - 2045, May 2023.
[36] X. Ran, J. Zhang, W. Zhu, *et al*, "A model of correlated interval-probabilistic conditional value-at-risk and optimal dispatch with spatial correlation of multiple wind power generations," *Int. J. Elect. Power Energy Syst.*, vol. 155, pp. 1 - 11, Jan. 2024.
[37] Z. Lin, H. Chen, J. Chen, *et al*, "Risk-averse robust interval economic dispatch for power systems with large-scale wind power integration," *CSEE J. Power Energy Syst.*, vol. 10, no. 1, pp. 105 - 116, Jan. 2024.
[38] X. Ran, W. P. Tay, and C. H. Lee, "Uncertain interval-based risk dispatch approach of power systems under an unified framework of multiple uncertainties," *IEEE Trans. Ind. Informat.*, vol.21, no.3, pp.2053 - 2063, Mar. 2025.
[39] Z. Wang, C. Shen, F. Liu, *et al*, "Chance-constrained economic dispatch with non-gaussian correlated wind power uncertainty," *IEEE Trans. Power Syst.*, vol.32, no.6, pp.4880 - 4893, Nov. 2017.
[40] M. Ortega-Vazquez and D. Kirschen, "Estimating the spinning reserve requirements in systems with significant wind power generation penetration," *IEEE Trans. Power Syst.*, vol.24, no.1, pp.114 - 124, Feb. 2009.
[41] X. Ran, W. P. Tay, and C. H. Lee, "High-performance optimization model based on novel conditional value at risk metric for power grids with high wind power penetration," *IEEE Trans. Ind. Informat.*, vol.21, no.7, pp.5689 - 5700, Jul. 2025.
[42] A. Vaccaro, C. Cañizares, and K. Bhattacharya, "A range arithmetic-based optimization model for power flow analysis under interval uncertainty," *IEEE Trans. Power Syst.*, vol. 28, no. 2, pp. 1179 - 1186, May 2013.

Xiaohong Ran (Member, IEEE) received the Ph.D. degree in electrical power engineer from Huazhong University of Science and Technology, Wuhan, China, in 2015.

Since 2015, he has been with the school of Electrical Engineering and Automation in Wuhan University, Wuhan, China. Now he is with Department of Electrical and Electronic Engineering, The Hong Kong Polytechnic University, Hong Kong. From 2018 to 2021, he was a Visiting Researcher with the School of Electrical and Computer Engineering, Georgia Institute of Technology, Atlanta, USA. From 2021 to 2023, he was a Senior Research Fellow at the Energy Research Institute, Nanyang Technological University, Singapore. His research interests include the modeling and control of networked AC and DC power grids, risk quantification, stability and resiliency of smart grids with high penetration of DERs, and artificial intelligence based state estimation, security defense and resilience control in cyber-physical power systems.

Siqi Bu (Senior Member, IEEE) received the Ph.D. degree in power system stability analysis from the electric power and energy research cluster, The Queen's University of Belfast, Belfast, U.K.

He continued the Postdoctoral Research work before entering into industry with The Queen's University of Belfast. He was an experienced U.K. National Transmission System Planner and Operator with National Grid U.K., London, U.K. He is currently a Professor and an Associate Head with the Department of Electrical and Electronic Engineering, The Hong Kong Polytechnic University, Kowloon, Hong Kong, an Associate Director of Research Centre for Grid Modernisation, and a Chartered Engineer with U.K. Royal Engineering Council, London. His research interests include power system stability, operation and economics considering renewable energy integration, smart grid application, and transport electrification.

Dr Bu is the Editor of IEEE TRANSACTIONS ON POWER SYSTEMS, IEEE TRANSACTIONS ON CONSUMER ELECTRONICS, IEEE POWER ENGINEERING LETTERS, IEEE OPEN ACCESS JOURNAL OF POWER AND ENERGY, CSEE Journal of Power and Energy Systems, Protection and Control of Modern Power Systems, Journal of Modern Power Systems and Clean Energy, and Advances in Applied Energy. He is a Fellow of IET, Chairman of IET HK Power and Energy Section, Co-Chairman of IET DPSP 2025 and APSCOM 2025, and Technical Chairman of IEEE PESIM 2026.